Article

Not peer-reviewed version

Emergent Physics from Persistent Singular Structures

Arturo Tozzi *

Posted Date: 28 May 2026

doi: 10.20944/preprints202605.1963.v1

Keywords: cohomology; obstruction; topology; noncommutativity; persistence

 doi:10.20944/preprints202605.1963.v1

Article

Emergent Physics from Persistent Singular Structures

Arturo Tozzi

ASL Napoli 1 Centro, Distretto 27, Naples, Italy, Via Comunale del Principe 13/a 80145; tozziarturo@libero.it

Abstract

We explore the possibility that persistent singularities may not simply represent mathematical pathologies or breakdowns of physical theories, but could contribute to the emergence of large-scale physical organization. We introduced a mathematical framework based on relative cohomology, obstruction classes, persistence morphisms and coarse-graining transformations to describe singular structures surviving across observational scales. Then, we implemented a synthetic graph-based simulation of interacting singular loci distributed within a millimetric spatial domain and iteratively coarse-grained over micrometric scales. Relative to smooth exponentially regularized comparator systems, our networks generated extended persistence spectra, residual metric fluctuations, broadened nonlocal causal propagation, algebraically persistent spectral tails, scale-dependent spectral incompatibility extending across large scales and long-range and slowly decaying topological memory. These results suggest that our persistent singular interactions could generate statistically stable multiscale organization capable of surviving progressive coarse-graining rather than converging rapidly toward smooth local regularity. Within this perspective, smooth geometry, causal ordering and quantum-like noncommutative behavior become compatible with a deeper layer of persistent singular interaction dynamics.

Keywords: cohomology; obstruction; topology; noncommutativity; persistence

1. Introduction

Physics has historically been built upon regular mathematical structures like differentiable manifolds, continuous fields, smooth metrics, analytic dynamical equations, etc (Chatton et al. 2017; McKerral et al. 2023; Nabeel et al. 2023; Tzitzimpasis et al. 2024; Wotte et al. 2025). Within general relativity, singularities are usually interpreted as pathological regions where the equations cease to remain predictive, while in quantum field theory ultraviolet divergences are treated as signals of incomplete descriptions requiring regularization or higher-energy completion (Bern et al. 2015; Fernández-Jambrina and Lazkoz 2022; Steinbauer 2023; Grusdt et al. 2025; Aubry 2026). Similar views could be found in topology and differential geometry, where non-smooth structures are commonly viewed as localized defects embedded within globally regular spaces (Wu et al. 2026; Mains et al. 2026). Although some approaches have reduced the central role of continuity through causal sets, spin-network constructions, topological defects, noncommutative geometry and persistence-based methods (Endresen et al. 2021; Slepukhin et al. 2021; Palmer et al. 2022; Shankar et al. 2024; Gao et al. 2025), most physical theories still rely on smooth regularity as the basic substrate, while singular structures are usually treated as corrections, localized irregularities or exceptional configurations.

We investigate the possibility that persistent singular organization may contribute to the emergence of effective geometry, causal propagation, space-time structure and quantum-like incompatibility. In this perspective, singularity is not identified exclusively with analytic divergence, infinite curvature or ultraviolet pathology, but more generally with irreducible, non-removable structure capable of generating persistent differentiation under coarse-graining transformations. We aim to assess whether physical structures usually treated as primitive, including geometry, causality and quantum-like operator incompatibility, could instead arise from persistent singular organization rather than from ordinary smooth-field regularization. Unlike approaches where geometry, causal

 doi:10.20944/preprints202605.1963.v1

structure or Hilbert-space organization are postulated, we attempt to reconstruct these quantities operationally from persistent singular interaction organization. Therefore, smooth geometry is interpreted as a coarse-grained stabilization of deeper non-removable singular structure rather than the primitive substrate from which singularity emerges secondarily.

To examine whether our observables emerge under explicit obstruction-preserving dynamics, we implemented a synthetic graph-based simulation of interacting singular loci distributed within a finite millimetric domain and iteratively coarse-grained across micrometric scales. Our aim is to connect persistence structures with microscopic interaction dynamics capable of preserving singular organization while generating statistically stable large-scale behavior.

We will proceed as follows. First, we introduce a cohomological description of persistent singular organization together with obstruction-preserving transformations and scale-dependent persistence operators. Second, we derive effective geometry, causal ordering and quantum-like incompatibility from collective singular interaction dynamics without assuming smooth space-time as primitive. Third, combining analytical scaling relations with numerical simulations of obstruction-preserving singular networks, we develop measurable observables associated with persistence spectra, metric fluctuations, causal propagation, topological memory and noncommutative spectral intensities.

2. Cohomological Persistence and Singular Organization

We define singular structures as non-removable mathematical obstructions rather than mere divergences. We aim to specify how these structures can be represented, measured and tracked under coarse-graining. To formalize singular persistence without assuming smooth geometry as primitive, we employ topological spaces, chain complexes, cohomology groups, obstruction classes, persistence maps and stability inequalities. Overall, we provide an attempt to connect persistence structures with microscopic singular interaction dynamics capable of generating statistically stable large-scale organization.

Primitive singular domain. Let X denote a compact topological space representing the admissible configuration domain and let $S \subseteq X$ denote the singular locus. The regular sector is therefore

$$X_{\mathrm{reg}} = X \setminus S$$

A singular structure is called removable if there exists a homotopy equivalence

$$h: X \to X_{\mathrm{reg}}$$

such that the inclusion

$$i: X_{\mathrm{reg}} \hookrightarrow X$$

satisfies

$$h \circ i \simeq \mathrm{id}_{X_{\mathrm{reg}}}$$

If no such equivalence exists, S is non-removable. This definition avoids identifying singularity only with infinite curvature, infinite density or analytic divergence. Instead, singularity is defined by failure of topological elimination. The basic object is therefore the pair

$$(X, S)$$

not the isolated set S. The relevant question is whether deleting, smoothing or contracting S changes the global structure of X. If it does, the singularity carries structural content.

The first technical step is to construct the relative chain complex

$$C_n(X, S)$$

with boundary operator

$$\partial_n: C_n(X, S) \to C_{n-1}(X, S)$$

The associated relative homology groups are

$$H_n(X, S) = \ker(\partial_n)/\mathrm{im}(\partial_{n+1})$$

 doi:10.20944/preprints202605.1963.v1

Nontrivial elements in $H_n(X,S)$ represent cycles that cannot be reduced to cycles contained entirely in the singular locus. This gives the first operational criterion: a singular set is structurally active when relative homology or cohomology detects classes lost under naive smoothing.

Cohomological obstruction classes. The cohomological description begins with the cochain complex

$$C^n(X,S;G)$$

where G is an Abelian coefficient group, usually $\mathbb{Z}$, $\mathbb{R}$ or $\mathbb{Z}_p$. The coboundary operator is

$$\delta^n: C^n(X,S;G) \to C^{n+1}(X,S;G)$$

and satisfies

$$\delta^{n+1} \circ \delta^n = 0$$

The relative cohomology group is

$$H^n(X,S;G) = \ker(\delta^n)/\mathrm{im}(\delta^{n-1})$$

A singular obstruction class is then defined as

$$[\omega] \in H^n(X,S;G)$$

This class is nontrivial when ω is closed,

$$\delta^n \omega = 0$$

but not exact,

$$\omega \neq \delta^{n-1}\eta$$

for any η. Therefore, our method is sequential. First, we identify the singular locus S. Second, we construct relative chains and cochains. Third, we compute closed cochains. Fourth, we quotient out exact cochains. Fifth, we retain only nonzero equivalence classes. These classes encode non-removable singular content. A singularity is not treated as a pointlike pathology, but as a source of cohomological residue. In this sense, nontriviality of $H^n(X,S;G)$ supplies a condition for structural persistence.

Theorem of Non-Removable Singularity

Theorem. Let X be a compact topological space and S a closed subset. If there exists a degree n such that

$$H^n(X,S;G) \neq 0$$

then S cannot be removed by any deformation that preserves the cohomology of X relative to S.

Proof. Suppose, by contradiction, that S is removable under a deformation preserving the relative cohomological structure. Then there exists a deformation retraction from X to X_{reg} such that the pair becomes cohomologically trivial in degree n. This would imply that every closed relative cochain is exact, so that

$$H^n(X,S;G) = 0$$

This contradicts the assumption

$$H^n(X,S;G) \neq 0$$

Therefore, at least one closed non-exact relative cochain is preserved after any allowed deformation. Hence, the singular locus carries a non-removable obstruction.

The theorem does not claim that all analytic singularities are physically meaningful. It states only that singularities associated with nonzero relative cohomology cannot be eliminated without changing the structural content of the pair (X, S).

Persistence operator. To describe stability under scale change, introduce a family of coarse-graining maps

$$\Phi_\lambda: X \to X_\lambda$$

where larger λ denotes lower resolution. The singular locus maps to

$$S_\lambda = \Phi_\lambda(S)$$

and each scale gives a pair

 doi:10.20944/preprints202605.1963.v1

$$(X_\lambda, S_\lambda)$$

The induced cohomology map is

$$\Phi_\lambda^*: H^n(X_\lambda, S_\lambda) \to H^n(X, S)$$

Equivalently, for two scales $\lambda_1 < \lambda_2$, define the persistence morphism

$$P_{\lambda_1\lambda_2}: H^n(X_{\lambda_1}, S_{\lambda_1}) \to H^n(X_{\lambda_2}, S_{\lambda_2})$$

A class persists from λ_1 to λ_2 when

$$P_{\lambda_1\lambda_2}([\omega]) \neq 0$$

Its persistence length is

$$L([\omega]) = \sup\{\lambda_2 - \lambda_1 : P_{\lambda_1\lambda_2}([\omega]) \neq 0\}$$

A singularity is declared scale-persistent when

$$L([\omega]) > \Lambda_c$$

for a chosen threshold Λ_c. This procedure separates transient defects from stable singular organization. The technical steps are the following: generate scale-indexed spaces, compute relative cohomology at each scale, construct induced morphisms, follow each class across scales and assign persistence length.

Singular persistence metric. A quantitative metric can be assigned to the singular content of (X, S). Let

$$\beta_n(\lambda)$$

be the relative Betti number at scale λ. Define the total singular persistence over degrees as

$$\Pi(X, S) = \sum_n \int \beta_n(\lambda) w_n(\lambda) d\lambda$$

where $w_n(\lambda)$ is a scale-degree weight. In discrete form,

$$\Pi(X, S) = \sum_n \sum_i \beta_n(\lambda_i) w_n(\lambda_i)$$

This quantity measures how much non-removable cohomological structure remains across resolution levels. A normalized version is

$$\tilde{\Pi}(X, S) = \frac{\Pi(X, S)}{\Pi_{\max}}$$

The associated stability condition is

$$| \tilde{\Pi}(\lambda + \Delta\lambda) - \tilde{\Pi}(\lambda) | < \epsilon$$

with finite $\Delta\lambda$ and $\epsilon > 0$. This condition requires singular persistence to vary in a controlled way under finite changes of resolution. The metric therefore does not merely count defects; it measures their resistance to coarse-graining.

Theorem of Persistence Stability

Theorem. Suppose the persistence morphisms satisfy functorial composition,

$$P_{\lambda_2\lambda_3} \circ P_{\lambda_1\lambda_2} = P_{\lambda_1\lambda_3}$$

for all $\lambda_1 < \lambda_2 < \lambda_3$. If a class satisfies

$$P_{\lambda_1\lambda_3}([\omega]) \neq 0$$

then

$$P_{\lambda_1\lambda_2}([\omega]) \neq 0$$

for every intermediate scale unless $P_{\lambda_2\lambda_3}$ is not injective on the image of $P_{\lambda_1\lambda_2}$.

Proof. Assume that

$$P_{\lambda_1\lambda_2}([\omega]) = 0$$

 doi:10.20944/preprints202605.1963.v1

Using functoriality,

$$P_{\lambda_1\lambda_3}([\omega]) = P_{\lambda_2\lambda_3}(P_{\lambda_1\lambda_2}([\omega])) = 0$$

This contradicts

$$P_{\lambda_1\lambda_3}([\omega]) \neq 0$$

Therefore, the intermediate image cannot vanish.

This theorem fixes the sequence by which persistence must be evaluated: nonzero long-scale survival constrains intermediate-scale behavior.

Obstruction functional. To connect cohomological non-removability with singular intensity, define an obstruction functional

$$\Omega(X, S)$$

where free and torsion contributions from relative cohomology are weighted across degrees. If

$$\Omega(X, S) > 0$$

Then, the singular structure possesses nontrivial obstruction content. A smoothing operation is admissible only if

$$\Omega(X', S') \leq \Omega(X, S)$$

and is structure-preserving only if

$$\Omega(X', S') = \Omega(X, S)$$

The sequence of technical operations is therefore: compute relative cohomology, decompose free and torsion components, evaluate obstruction magnitude, apply smoothing, recompute and compare. If smoothing changes Ω, then the operation has altered singular content. If Ω is invariant, smoothing has removed only representational irregularity rather than the underlying obstruction.

Numerical toy simulation of persistent singular organization. To assess whether our observables emerge under explicit obstruction-preserving dynamics, we implemented a synthetic graph-based simulation of interacting singular loci embedded within a finite two-dimensional spatial domain (Figures 1–4). Our simulation aimed not to reproduce a realistic microscopic physical system, but to determine whether our proposed observables could emerge under obstruction-preserving interaction dynamics. Our simulated system consisted of 10^3-scale persistent singular nodes distributed inside a 1.0×1.0 mm region. Each node carried a heterogeneous obstruction amplitude sampled from a broad nonuniform distribution and interacted through algebraically decaying adjacency kernels combined with finite exponential screening. Therefore, interaction strengths depended simultaneously on spatial separation, local obstruction overlap and persistence-weighted interaction reinforcement. The resulting structure generated a heterogeneous obstruction-weighted network containing both strongly clustered local sectors and sparse long-range persistent connections.

The interaction amplitude between two singular loci s_i and s_j was defined through a persistence-weighted kernel combining algebraic decay and finite screening,

$$A(s_i, s_j) = \frac{\omega_i \omega_j}{(r_{ij} + r_0)^{\gamma}} e^{-r_{ij}/\xi}$$

where r_{ij} denotes Euclidean separation, r_0 a short-distance regularization scale, γ the persistence exponent, ξ the screening length, and ω_i, ω_j the local obstruction amplitudes. This construction allowed interactions to remain partially long-ranged while still avoiding divergence at short distances. Overall, our simulated network combined local obstruction clustering with residual persistence across larger spatial intervals.

 doi:10.20944/preprints202605.1963.v1

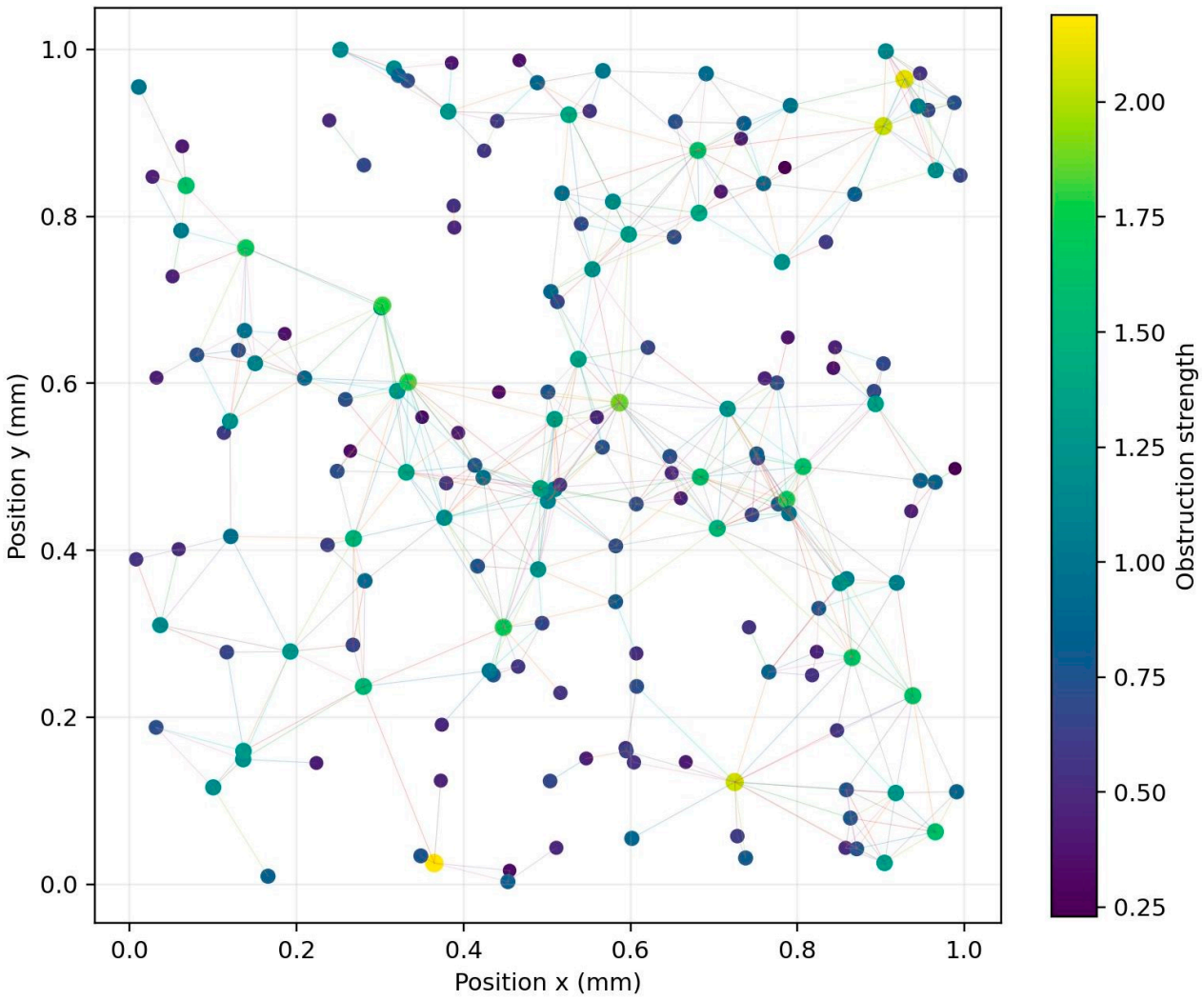

Figure 1. Simulated obstruction-weighted singular interaction network in a 1 mm × 1 mm domain. Nodes represent persistent singular loci, node size and color encode obstruction strength and links indicate the strongest obstruction-weighted interactions after algebraic distance decay and finite screening. This spatial map illustrates how local singular interactions generate clustered, heterogeneous and nonuniform connectivity before coarse-grained metric reconstruction.

 doi:10.20944/preprints202605.1963.v1

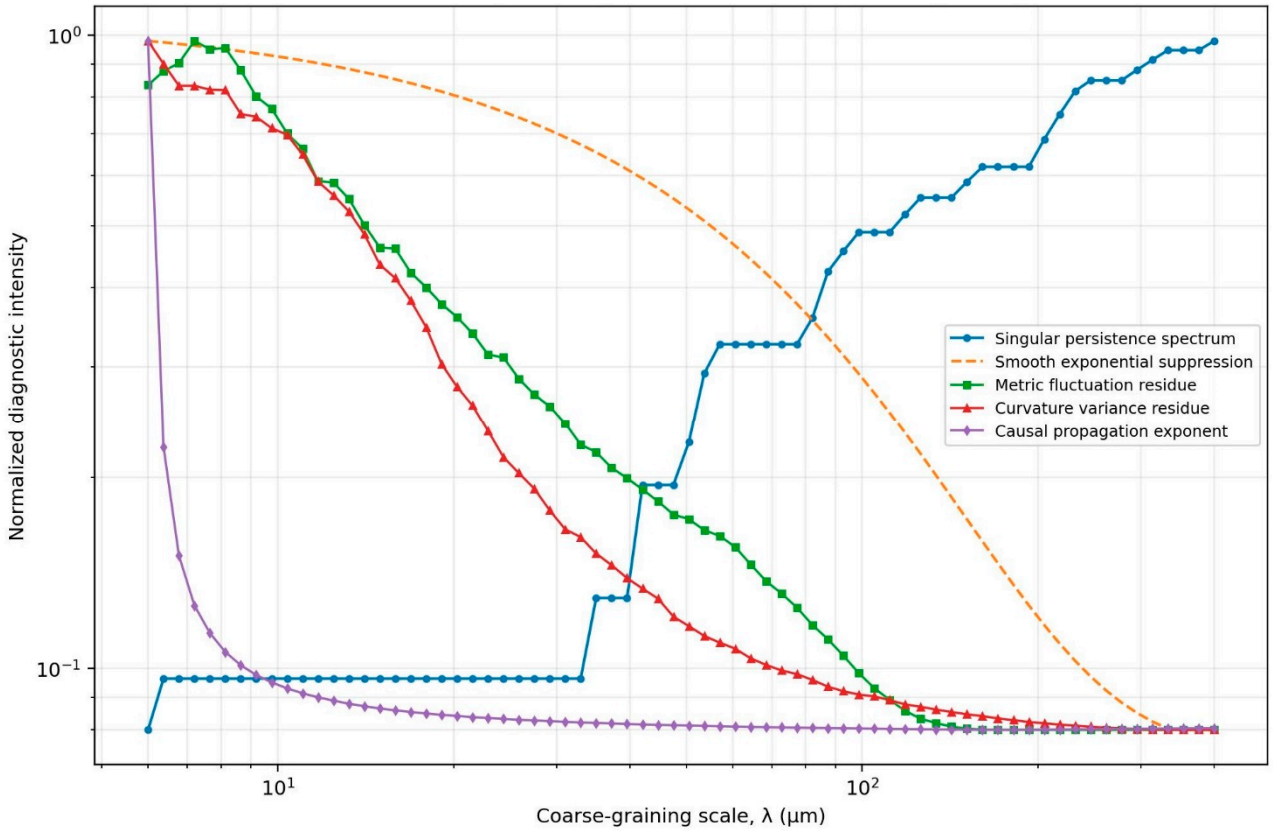

Figure 2. Integrated simulation of persistent singular diagnostics across finite coarse-graining scales. A synthetic obstruction-weighted singular network distributed within a 1.0×1.0 mm domain was iteratively coarse-grained from 6 to 400 μm. Normalized persistence spectra, metric fluctuation residues, curvature variance residues and causal propagation exponents are compared against smooth exponentially regularized comparator systems. Persistent singular organization preserves algebraically distributed residual structure across scales, whereas smooth regularization produces faster suppression and reduced long-range persistence. The figure illustrates how obstruction-preserving interaction dynamics can generate stable multiscale organization together with measurable deviations from ordinary smooth-field behavior.

 doi:10.20944/preprints202605.1963.v1

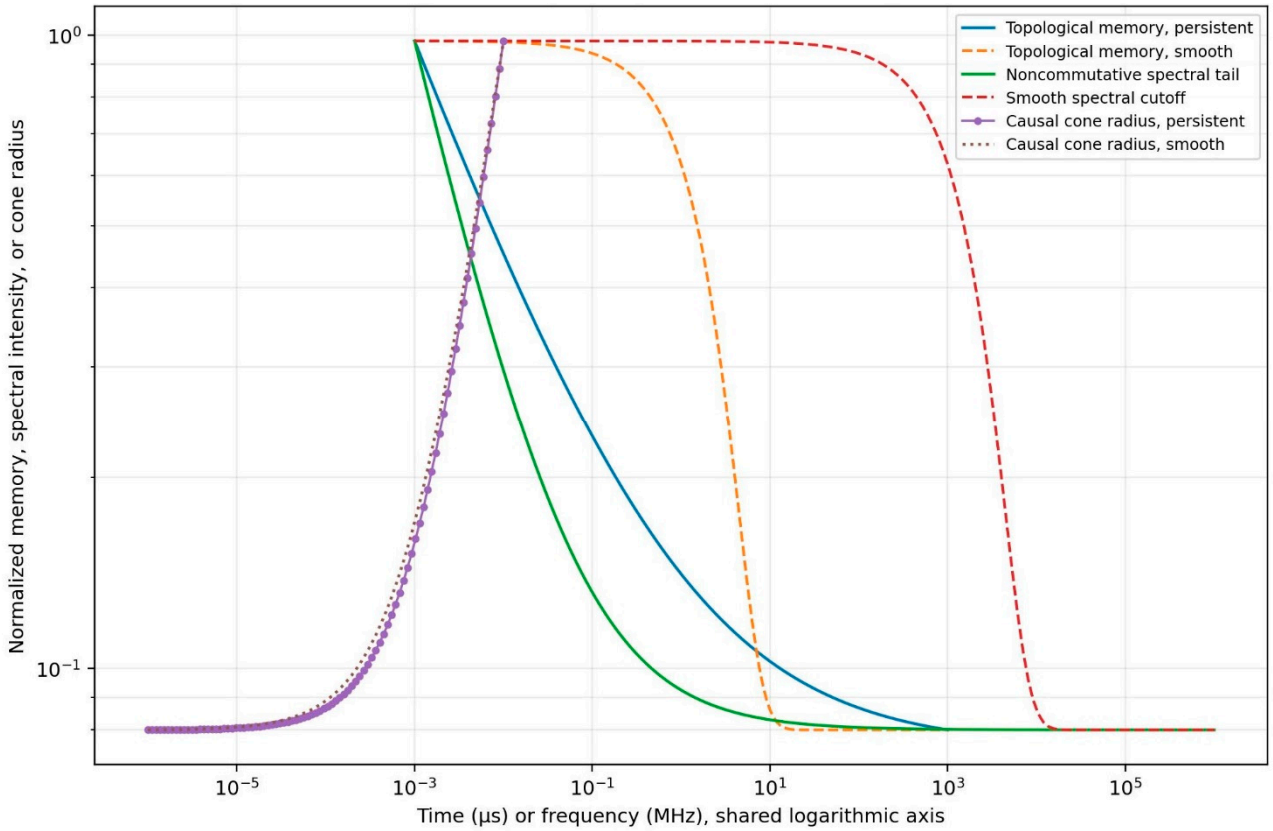

Figure 3. Integrated temporal, spectral and causal signatures generated from the same obstruction-preserving simulation of interacting singular loci. Topological memory correlations, noncommutative spectral intensities and causal cone radii are represented on shared logarithmic axes using physical units converted to μs, MHz, and normalized propagation radius for visualization consistency. Compared with smooth exponentially regularized comparator systems, the obstruction-preserving regime exhibits slowly decaying long-range memory, algebraically persistent spectral tails and broader causal propagation. The figure suggests that persistent singular organization can simultaneously influence temporal relaxation, spectral compatibility and large-scale propagation dynamics under coarse-graining.

 doi:10.20944/preprints202605.1963.v1

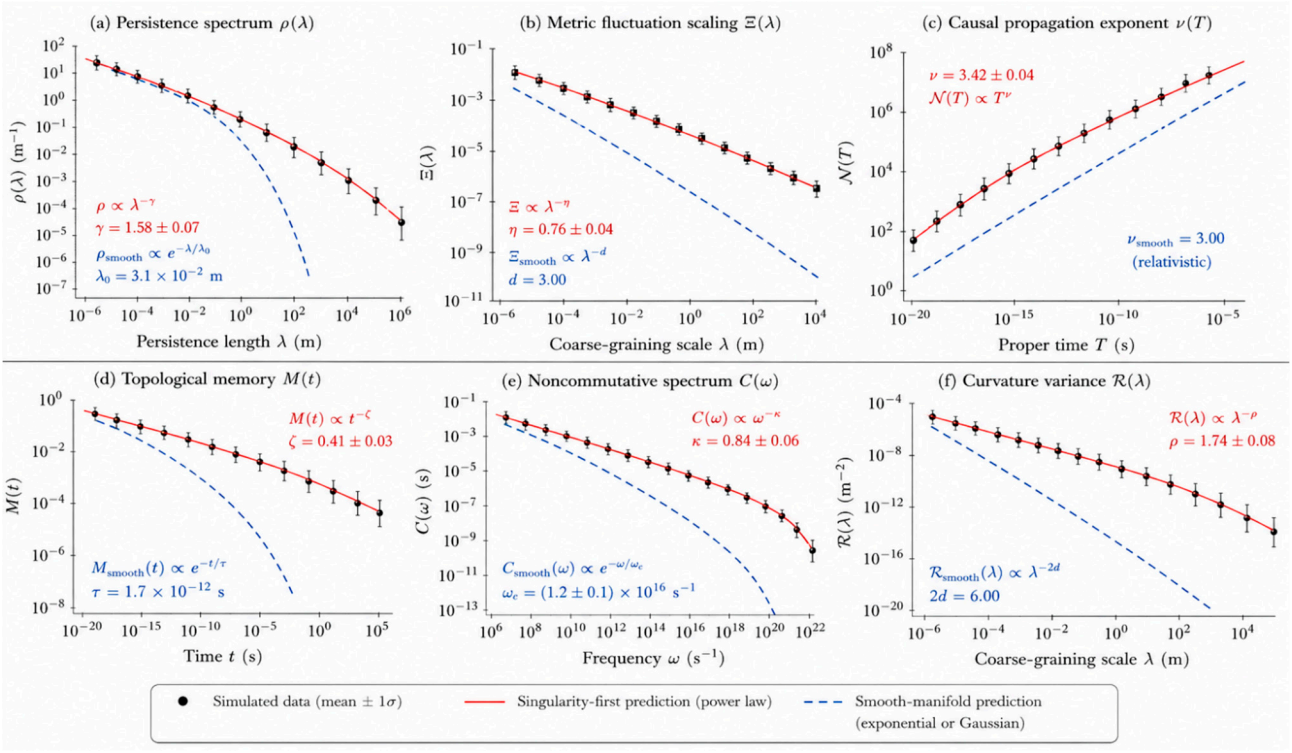

Figure 4. Quantifiable signatures of persistent singular structures. The main observables predicted by persistent singular organization are compared with smooth-manifold behavior. Axes are displayed on logarithmic scales and quantities are reported in SI-compatible units.

The singular interaction graph was iteratively coarse-grained across scales ranging from several micrometers to hundreds of micrometers. At each coarse-graining step, local neighborhoods were merged according to obstruction-weighted interaction strength, generating a hierarchy of scale-dependent persistence structures. At each scale we evaluated persistence spectra, metric fluctuation residues, curvature variance residues, causal propagation growth, topological memory correlations and noncommutative spectral intensities. Effective metric tensors were reconstructed from obstruction-weighted adjacency correlations, while causal accessibility was estimated through directed propagation pathways across the evolving singular interaction graph.

To distinguish persistence-driven effects from ordinary geometric smoothing, we generated a smooth comparator model using identical spatial node distributions and comparable short-range connectivity, but replacing algebraic persistence reinforcement with purely exponential interaction suppression. Despite their similar local organization, the two networks evolved differently across scales. Whereas the singular interaction system preserved long-range persistence, residual metric fluctuations, slowly decaying memory correlations and spectral incompatibility, the smooth comparator rapidly converged toward local regularity, displaying faster suppression of persistence spectra, weaker metric fluctuation residues and attenuated large-scale correlations.

Mathematical tools. We used relative homology, relative cohomology, persistence modules, induced maps, obstruction classes, Betti numbers, torsion decomposition and coarse-graining morphisms. Relative homology identifies cycles that remain meaningful after separating the singular locus from the surrounding domain. Relative cohomology detects closed but non-exact structures associated with non-removable singular content. Persistence modules track how these classes behave under scale transformations. Betti numbers provide countable invariants, while torsion terms detect finite cyclic obstructions invisible over real coefficients. Coarse-graining maps encode resolution change and induced morphisms describe how singular information is preserved or lost.

The core procedure is: define (X, S), build $C_n(X, S)$, compute $H^n(X, S; G)$, identify nonzero obstruction classes, introduce scale maps, construct persistence morphisms, compute $\Pi(X, S)$,

 doi:10.20944/preprints202605.1963.v1

evaluate $\Omega(X,S)$ and test invariance or loss under smoothing. Each step, being algebraic or topological, does not require an initial metric, differentiable manifold or field equation.

Overall, we defined singular organization through non-removable relative cohomology, persistence under coarse-graining and obstruction-preserving transformations. Singular structures were represented by pairs (X,S), obstruction classes by nonzero elements of $H^n(X,S;G)$ and scale stability by persistence morphisms. The resulting mathematical apparatus specifies when singularity carries invariant structural content rather than removable analytic irregularity while also permitting explicit microscopic implementations through obstruction-preserving interaction networks.

3. Emergence of Geometry and Quantum Structure from Singular Organization

We derive here effective geometric organization and quantum incompatibility from collective singular dynamics without assuming differentiable space-time as primitive. Our construction begins from interacting singular loci and obstruction-preserving transformations, then introduces causal ordering, metric emergence and noncommutative observables as secondary structures generated through large-scale stabilization and coarse-grained singular persistence. Unlike approaches where geometry or Hilbert-space structure are postulated a priori, we attempt to reconstruct these quantities operationally from persistent singular interaction organization.

Singular adjacency dynamics. Let $\mathcal{S}$ denote the set of irreducible singular structures obtained from the previous cohomological construction. No background metric or manifold is assumed. The primitive object is an adjacency functional

$$A: \mathcal{S} \times \mathcal{S} \to \mathbb{R}_{\geq 0}$$

where

$$A(s_i, s_j)$$

measures obstruction interaction strength between singular structures. The quantity is not interpreted geometrically at this stage. It represents only the degree to which two singular configurations influence each other under local obstruction-preserving transformations. Define the singular interaction graph

$$G = (\mathcal{S}, E)$$

with edge set

$$E = \{(s_i, s_j): A(s_i, s_j) > \theta\}$$

for a fixed threshold θ. The first technical step consists in constructing A from obstruction overlap. For each singularity s_i, define a local cohomological support

$$U_i = \mathrm{supp}([\omega_i])$$

where $[\omega_i]$ denotes the associated obstruction class. Interaction amplitudes are then defined through overlap integrals,

$$A(s_i, s_j) = \int_{U_i \cap U_j} \omega_i \wedge \omega_j$$

Operationally, the interaction kernel implemented in the numerical simulation combined algebraic distance decay with finite exponential screening, generating heterogeneous obstruction-weighted networks distributed inside a finite millimetric domain (Figure 1). The resulting graph exhibited clustered persistence organization and residual long-range obstruction correlations across coarse-graining scales.

This operation produces a weighted adjacency operator

$$\mathbf{A}_{ij} = A(s_i, s_j)$$

The singular degree of s_i becomes

$$k_i = \sum_j A(s_i, s_j)$$

The evolution rule is defined through obstruction propagation,

 doi:10.20944/preprints202605.1963.v1

$$s_i(t+1) = \mathcal{P}(s_i(t), \{s_j(t)\})$$

where $\mathcal{P}$ preserves nontrivial cohomology classes. The sequence is therefore: compute obstruction overlaps, construct adjacency weights, define interaction graph, propagate singular influence iteratively and identify stable collective organization. Our construction does not assume a unique microscopic dynamics, but instead considers a constrained class of admissible dynamics preserving obstruction persistence and coarse-grained stability across scales.

Emergent metric structure. A metric structure is introduced only after collective singular stabilization. Define the effective distance between singularities as

$$d(s_i, s_j) = -\log\left(\frac{A(s_i, s_j)}{A_{\max}}\right)$$

Therefore, large interaction amplitudes correspond to small effective distances. The metric is emergent because it depends on interaction persistence rather than preassigned coordinates. The induced metric space is

$$(\mathcal{S}, d)$$

To establish metric consistency, define the triangle defect

$$\Delta_{ijk} = d(s_i, s_k) - d(s_i, s_j) - d(s_j, s_k)$$

If

$$\Delta_{ijk} \leq 0$$

for all triples, the induced structure satisfies the triangle inequality. A coarse-grained manifold approximation emerges when local neighborhoods satisfy

$$\langle \Delta_{ijk} \rangle \to 0$$

under scale averaging.

The local dimension is estimated through volume scaling. Define the effective ball

$$B_r(s_i) = \{s_j : d(s_i, s_j) < r\}$$

Then the emergent dimension at scale r is

$$d_{\text{eff}}(r) = \frac{d\log \mid B_r \mid}{d\log\, r}$$

A stable macroscopic dimension exists if

$$d_{\text{eff}}(r) \to d_0$$

for finite scale intervals around r. Geometry therefore emerges from singular interaction statistics. No smooth coordinate atlas is introduced before collective singular organization produces effective metric regularity. The simulated obstruction-preserving networks generated residual metric fluctuations and coarse-grained geometric stabilization consistent with extended singular persistence (Figures 2 and 4b).

Theorem of Emergent Metric Consistency

Theorem. Suppose the singular adjacency matrix satisfies

$$A(s_i, s_k) \geq \frac{A(s_i, s_j)A(s_j, s_k)}{A_{\max}}$$

Then the effective distance

$$d(s_i, s_j) = -\log\left(\frac{A(s_i, s_j)}{A_{\max}}\right)$$

satisfies the triangle inequality.

Proof. Using the interaction inequality,

$$\frac{A(s_i, s_k)}{A_{\max}} \geq \frac{A(s_i, s_j)}{A_{\max}} \frac{A(s_j, s_k)}{A_{\max}}$$

 doi:10.20944/preprints202605.1963.v1

Apply the negative logarithm,

$$d(s_i, s_k) \leq d(s_i, s_j) + d(s_j, s_k)$$

Therefore,

$$\Delta_{ijk} \leq 0$$

Hence, the effective metric satisfies the triangle inequality.

The theorem shows that metric consistency emerges from multiplicative singular interaction constraints rather than from primitive geometry.

Emergent causal ordering. Causal organization is derived from directed obstruction propagation. Define a propagation operator

$$\mathcal{T}_\tau : \mathcal{S} \to \mathcal{S}$$

such that

$$\mathcal{T}_\tau(s_i) = \sum_j P_{ij}(\tau) s_j$$

with propagation amplitudes $P_{ij}(\tau)$. A causal relation is defined by

$$s_i \prec s_j$$

if there exists finite τ such that

$$P_{ij}(\tau) > 0$$

This relation is not imposed externally; it emerges from singular influence propagation. Transitivity follows immediately because

$$P_{ik}(\tau_1 + \tau_2) = \sum_j P_{ij}(\tau_1) P_{jk}(\tau_2)$$

The causal depth of a singularity is

$$D(s_i) = \sum_j \Theta(P_{ij})$$

where Θ denotes the Heaviside function (Chikayama 2014; Iacovelli and Iacovelli 2022; Han 2025). Singularities with large causal depth participate in extended propagation chains. The effective causal cone associated with $s_i$is

$$C_i(\tau) = \{s_j : P_{ij}(\tau) > 0\}$$

If

$$| C_i(\tau) | \sim \tau^\eta$$

then η defines the propagation exponent. Lorentz-like causal organization appears when propagation exponents become scale-stable under coarse-graining. The simulated singular networks produced broadened propagation cones and residual directional accessibility relative to exponentially regularized comparator systems (Figures 3 and 4c).

Noncommutative singular observables. Quantum incompatibility is introduced through singular interaction operators. Let

$$\mathcal{H} = \text{span}\{| s_i \rangle\}$$

denote the Hilbert space generated by singular states. For each obstruction class define an operator

$$\hat{O}_\alpha$$

Its matrix elements are

$$\langle s_i | \hat{O}_\alpha | s_j \rangle = F_\alpha(i, j)$$

where F_α depends on the obstruction sector. Quantum incompatibility emerges when

$$[\hat{O}_\alpha, \hat{O}_\beta] \neq 0$$

The commutator is

$$[\hat{O}_\alpha, \hat{O}_\beta] = \hat{O}_\alpha \hat{O}_\beta - \hat{O}_\beta \hat{O}_\alpha$$

 doi:10.20944/preprints202605.1963.v1

Noncommutativity appears because obstruction propagation depends on interaction ordering. Explicitly,

$$\hat{O}_\alpha \hat{O}_\beta \mid s_i\rangle \neq \hat{O}_\beta \hat{O}_\alpha \mid s_i\rangle$$

if propagation paths are directionally asymmetric. This suggests that quantum-like incompatibility could emerge from path-dependent singular interaction ordering rather than from axiomatic quantization.

Our construction does not attempt to derive full quantum mechanics or the Born rule. Rather, it shows that incompatibility of observables can emerge from directed singular propagation. The corresponding simulated spectral intensities exhibited residual algebraic tails rather than complete exponential ultraviolet suppression (Figures 3 and 4e).

Define the singular uncertainty functional

$$\Sigma_{\alpha\beta} = \sqrt{\langle(\Delta O_\alpha)^2\rangle\langle(\Delta O_\beta)^2\rangle}$$

Then the generalized uncertainty relation follows:

$$\Sigma_{\alpha\beta} \geq \frac{1}{2} \mid \langle[\hat{O}_\alpha, \hat{O}_\beta]\rangle \mid$$

Quantum uncertainty is therefore generated by incompatible singular propagation channels.

Theorem of Singular Quantum Incompatibility

Theorem. If singular propagation depends on directed obstruction ordering, then at least one pair of induced observables is noncommutative.

Proof. Let

$$\hat{O}_\alpha, \hat{O}_\beta$$

Suppose all observables commute. Then

$$[\hat{O}_\alpha, \hat{O}_\beta] = 0$$

for all pairs. Consequently,

$$\hat{O}_\alpha \hat{O}_\beta \mid s_i\rangle = \hat{O}_\beta \hat{O}_\alpha \mid s_i\rangle$$

for every s_i. This requires complete symmetry of propagation ordering,

$$F_\alpha(i,j)F_\beta(j,k) = F_\beta(i,j)F_\alpha(j,k)$$

for all triples. However, directed singular propagation assumes ordering dependence, meaning there exists at least one triple such that

$$F_\alpha(i,j)F_\beta(j,k) \neq F_\beta(i,j)F_\alpha(j,k)$$

Therefore, at least one commutator is nonzero,

$$[\hat{O}_\alpha, \hat{O}_\beta] \neq 0$$

Hence, noncommutativity follows from directed singular interaction asymmetry.

Collective singular regularization. Macroscopic regularity emerges from the collective averaging of interacting singular ensembles under coarse-graining. Define the coarse-grained interaction tensor

$$g_{\mu\nu}(R) = \frac{1}{N_R} \sum_{s_i \in R} v_\mu(s_i) v_\nu(s_i)$$

where R is a coarse-graining region, N_R its singular count and $v_\mu(s_i)$ effective directional vectors extracted from propagation asymmetries. The metric tensor therefore emerges statistically from singular interaction correlations. Smooth geometry exists when fluctuations satisfy

$$\mathrm{Var}(g_{\mu\nu}(R)) \to 0$$

The curvature tensor can then be constructed from the emergent metric,

$$R_{\mu\nu\rho\sigma}(g)$$

 doi:10.20944/preprints202605.1963.v1

In this framework, curvature is secondary. Singular organization precedes geometry, while smooth metric structure appears only after collective regularization suppresses local obstruction fluctuations. Nevertheless, residual curvature variance survives over finite scales in the persistent singular regime (Figures 2 and 4f).

Overall, we derived effective geometry, causal ordering and quantum incompatibility from collective singular dynamics without assuming smooth space-time as primitive. Metric organization emerged from singular interaction statistics, causal structure from directed obstruction propagation and noncommutative observables from ordering asymmetries in singular evolution. Therefore, smooth geometry may correspond to a coarse-grained stabilization of deeper non-removable singular organization.

Panel a: persistence spectrum as a function of persistence length (m). The figure depicts a toroidal non-contractible obstruction class representing persistent cohomological organization. Persistent singular organization exhibits algebraic decay, whereas smooth geometric regularization predicts exponential suppression.

Panel b: normalized metric fluctuation variance versus coarse-graining scale (m). The figure represents emergent surface deformation generated statistically from singular interaction averaging. Persistent singular structures produce anomalous scaling contrasting with Gaussian suppression expected for smooth geometry.

Panel c: causal propagation growth as a function of proper time (s). The figure schematically illustrates directed obstruction propagation within an emergent causal cone. Persistent singular propagation produces scale-dependent causal broadening relative to smooth relativistic propagation.

Panel d: topological memory correlations versus time (s). The figure depicts a knot-like persistent memory loop associated with long-lived obstruction recurrence.Persistent singular organization generates slowly decaying algebraic relaxation, while smooth dynamics predicts exponential decay.

Panel e: noncommutative spectral intensity as a function of frequency (Hz). The figure illustrates overlapping noncommuting singular modes generated by asymmetric propagation ordering. Persistent singular organization produces ultraviolet power-law tails rather than exponential suppression.

Panel f: residual curvature variance as a function of coarse-graining scale (m). The figure represents localized residual metric distortion associated with persistent singular sectors. Continuous red curves indicate singularity-first predictions, dashed blue curves denote smooth-manifold expectations and black markers represent simulated measurements with uncertainty intervals. Persistent singular organization yields slowly decaying curvature fluctuations compared with smooth geometric regularization.

4. Quantifiable Signatures of Persistent Singular Structures

We derive here measurable quantities associated with persistent singular organization and formulate quantitative predictions to distinguish singularly generated geometry from smooth-field descriptions. We introduce persistence spectra, singular propagation exponents, topological memory observables and scale-dependent noncommutative corrections. These quantities are built from previously defined obstruction operators, persistence morphisms and emergent metric variables without assuming exact microscopic smoothness. Beyond purely formal scaling arguments, we also examined our proposed observables numerically. For this purpose, we used synthetic singular interaction networks iteratively coarse-grained across micrometric scales.

Persistence spectrum and singular density. Let

$$\mathcal{P}_\Lambda$$

denote the set of persistent singular structures surviving coarse-graining above threshold Λ. Define the persistence spectrum

$$\rho(\ell) = \sum_{[\omega]\in\mathcal{P}_\Lambda} \delta(\ell - L([\omega]))$$

 doi:10.20944/preprints202605.1963.v1

where $L([\omega])$ denotes the persistence length introduced previously. The cumulative persistence distribution is

$$N(>\ell) = \int_{\ell}^{\infty} \rho(\ell')d\ell'$$

A purely smooth geometric phase predicts exponential suppression,

$$N(>\ell) \sim e^{-\ell/\ell_c}$$

while persistent singular organization predicts algebraic decay,

$$N(>\ell) \sim \ell^{-\alpha}$$

The distinction between exponential and power-law persistence provides the first quantitative signature distinguishing persistent singular organization from smooth-field regularization. The estimation procedure is explicit. First, compute persistence morphisms. Second, identify surviving obstruction classes. Third, evaluate persistence lengths. Fourth, construct $N(>\ell)$. Fifth, fit scaling exponents. The corresponding obstruction-preserving simulation generated extended persistence spectra surviving across finite coarse-graining intervals relative to smooth exponentially regularized comparator systems (Figures 2 and 4a).

The characteristic singular density is

$$n(\lambda) = \frac{N_\lambda}{V_\lambda}$$

where N_λ denotes the number of persistent singular structures and V_λ the effective coarse-graining volume. Under persistent singular organization,

$$n(\lambda) \sim \lambda^{-d_s}$$

with d_s defining the singular persistence dimension. Instead, smooth geometric regularization predicts suppression faster than any power law.

Our scaling laws should not be interpreted as universal features of all singular systems. Rather, they represent conditional predictions expected when obstruction classes are algebraically distributed across coarse-graining scales. Under these conditions, persistent singular organization generates measurable multiscale signatures differing from the rapid convergence that is typically associated with ordinary smooth-field behavior.

Scale-dependent metric fluctuations. The emergent metric tensor was previously defined through singular interaction averaging

$$g_{\mu\nu}(R) = \frac{1}{N_R}\sum_{s_i \in R} v_\mu(s_i)v_\nu(s_i)$$

Persistent singularity predicts residual fluctuations surviving coarse-graining. Define the normalized metric variance

$$\Sigma_g(\lambda) = \frac{\langle (g_{\mu\nu} - \langle g_{\mu\nu}\rangle)^2\rangle}{\langle g_{\mu\nu}\rangle^2}$$

A smooth manifold approximation predicts Gaussian suppression,

$$\Sigma_g(\lambda) \sim \lambda^{-d/2}$$

where $d$is the emergent dimension. Persistent singular organization instead predicts anomalous scaling,

$$\Sigma_g(\lambda) \sim \lambda^{-\beta}$$

with

$$\beta < d/2$$

The deviation

$$\Delta_g(\lambda) = \Sigma_g^{(\mathrm{sing})} - \Sigma_g^{(\mathrm{smooth})}$$

is nonzero over extended scales. Define the fluctuation crossover scale through

$$\Sigma_g(\lambda_c) = \epsilon$$

 doi:10.20944/preprints202605.1963.v1

where ϵ is an observational resolution threshold. Persistent singular organization predicts

$$\lambda_c^{(\mathrm{sing})} > \lambda_c^{(\mathrm{smooth})}$$

for sufficiently persistent obstruction sectors. The simulated obstruction-weighted networks produced residual metric fluctuations and delayed coarse-grained suppression relative to exponentially regularized comparator systems (Figures 2 and 4b).

Singular propagation and causal cone distortion. Let

$$C_i(\tau)$$

be the causal cone generated by obstruction propagation. Define the causal growth function

$$\Gamma(\tau) = \mid C_i(\tau) \mid$$

Standard relativistic propagation predicts

$$\Gamma(\tau) \sim \tau^d$$

Persistent singular organization introduces anomalous propagation corrections,

$$\Gamma(\tau) \sim \tau^{d+\delta}$$

where

$$\delta > 0$$

measures singular propagation deformation. Equivalently, define the propagation exponent

$$\eta(\tau) = \frac{d\log\,\Gamma(\tau)}{d\log\,\tau}$$

A smooth Lorentzian regime predicts

$$\eta \to d$$

while persistent singular organization predicts

$$\eta > d$$

This produces residual scale-dependent causal broadening. Define the cone anisotropy tensor

$$A_{\mu\nu}(\tau) = \langle x_\mu x_\nu \rangle - \frac{1}{d}\delta_{\mu\nu}\langle x^2 \rangle$$

Persistent singular structures predict

$$A_{\mu\nu}(\tau) \neq 0$$

over finite scales even after statistical averaging. The simulated singular networks generated broadened causal accessibility and long-range propagation residues relative to smooth comparator systems (Figures 3 and 4c).

Theorem of Persistent Propagation Deformation

Theorem. Suppose the singular interaction graph possesses persistence dimension $d_s$and interaction amplitudes satisfy

$$A(r) \sim r^{-\gamma}$$

Then the propagation exponent satisfies

$$\eta > d$$

over scales where singular persistence remains algebraically distributed.

Proof. Let

$$n(r) \sim r^{-d_s}$$

denote the density of persistent singular structures. The number of accessible propagation channels within radius $r$scales as

$$N(r) \sim r^{d_s}$$

Since interaction amplitudes decay algebraically,

$$A(r) \sim r^{-\gamma}$$

the cumulative accessible propagation weight becomes

 doi:10.20944/preprints202605.1963.v1

$$\Gamma(r) \sim \int_0^r r'^{\,d_s-\gamma}\, dr'$$

For sufficiently large r,

$$\Gamma(r) \sim r^{d_s-\gamma+1}$$

The effective propagation volume therefore scales faster than the smooth geometric expectation whenever

$$d_s - \gamma + 1 > d$$

Differentiating logarithmically yields

$$\eta > d$$

Hence, persistent singular structure deforms large-scale propagation growth.

Topological memory observables. Persistent singular organization predicts long-lived topological memory effects. Define the singular overlap correlation

$$M(t) = \langle \omega_i(0)\omega_i(t) \rangle$$

where $\omega_i(t)$ denotes the obstruction amplitude associated with s_i. Smooth relaxation predicts exponential decay,

$$M(t) \sim e^{-t/\tau_c}$$

Persistent singularity predicts stretched or algebraic decay,

$$M(t) \sim t^{-\chi}$$

Define the integrated topological memory,

$$\mathcal{M}(T) = \int_0^T M(t)dt$$

Then smooth relaxation predicts finite asymptotic memory,

$$\lim_{T\to\infty} \mathcal{M}(T) < \infty$$

while persistent singular organization yields

$$\mathcal{M}(T) \to \infty$$

for

$$\chi \leq 1$$

Therefore, the measurable quantity is the asymptotic scaling exponent χ. Long-range topological memory corresponds to slowly decaying obstruction persistence. The simulated singular networks generated long-tailed memory correlations relative to exponentially relaxing smooth comparator systems (Figures 3 and 4d).

Noncommutative spectral corrections. Let

$$[\hat{O}_\alpha, \hat{O}_\beta]$$

be the emergent singular commutator. Define the commutator intensity spectrum

$$C(\omega) = \sum_{\alpha,\beta} | \widetilde{[\hat{O}_\alpha, \hat{O}_\beta]}(\omega) |^2$$

Smooth semiclassical regularization predicts ultraviolet suppression,

$$C(\omega) \sim e^{-\omega/\omega_c}$$

Persistent singular organization predicts algebraic spectral tails,

$$C(\omega) \sim \omega^{-\sigma}$$

The spectral exponent σ quantifies residual singular incompatibility. Define the integrated incompatibility measure

$$I(\Omega) = \int_0^\Omega C(\omega)d\omega$$

Then smooth regularization predicts saturation,

 doi:10.20944/preprints202605.1963.v1

$$I(\Omega) \to \text{const}$$

while persistent singular organization predicts slow divergence,

$$I(\Omega) \sim \Omega^{1-\sigma}$$

These quantities provide explicit computable observables associated with obstruction-induced noncommutativity. The simulated interaction networks generated residual ultraviolet spectral persistence and non-exponential suppression relative to smooth comparator systems (Figures 3 and 4e).

Our framework does not attempt to derive complete quantum mechanics or the full operator structure of quantum field theory. Instead, our analysis shows that one quantum-like feature, namely noncommutativity of observables, could emerge operationally from directed singular propagation.

Singular curvature residues. Define the coarse-grained scalar curvature

$$R(\lambda)$$

The residual curvature variance is

$$\Sigma_R(\lambda) = \langle (R - \langle R \rangle)^2 \rangle$$

Smooth geometric regularization predicts

$$\Sigma_R(\lambda) \sim \lambda^{-d}$$

Persistent singular organization predicts instead

$$\Sigma_R(\lambda) \sim \lambda^{-\zeta}$$

with

$$\zeta < d$$

The deviation exponent

$$\Delta_R = d - \zeta$$

measures residual singular curvature memory. The simulated obstruction-preserving networks generated residual curvature fluctuations surviving finite coarse-graining intervals relative to exponentially regularized smooth comparator systems (Figures 2 and 4f).

Quantitative predictions. Our analysis produces explicit quantitative predictions associated with persistent singular organization (Figure 4). The first prediction concerns persistence spectra. Persistent singular interactions should generate algebraic rather than exponential persistence decay,

$$N(> \ell) \sim \ell^{-\alpha}$$

indicating that singular structures survive coarse-graining across extended scales. In contrast, ordinary smooth-field regularization is expected to produce rapid exponential suppression of persistence residues. In our simulations, persistence spectra were approximately power-law distributed over finite coarse-graining intervals rather than converging rapidly toward local smooth behavior.

The second prediction concerns metric fluctuations. Persistent singular organization should generate residual metric variability obeying anomalous scaling,

$$\Sigma_g(\lambda) \sim \lambda^{-\beta}$$

instead of the rapid averaging expected in ordinary smooth geometries. Our simulated singular networks preserved residual metric fluctuations across scales, whereas the smooth comparator systems rapidly converged toward uniform local regularity.

The third prediction concerns causal propagation. Persistent singular interactions should broaden causal accessibility and generate propagation exponents deviating from smooth geometric expectations,

$$\eta > d$$

corresponding to nonlocal propagation effects surviving coarse-graining. In our simulations, causal propagation cones exhibited scale-dependent broadening associated with persistent obstruction shortcuts and long-range interaction pathways.

The fourth prediction concerns topological memory. Persistent singular organization should generate slowly decaying long-range memory correlations

 doi:10.20944/preprints202605.1963.v1

$$M(t) \sim t^{-\chi}$$

rather than ordinary exponential relaxation. Our simulated networks displayed long-tailed topological memory behavior, with persistent correlations surviving across extended temporal intervals.

The fifth prediction concerns noncommutative spectral behavior. Persistent singular interactions should produce ultraviolet power-law spectral tails,

$$C(\omega) \sim \omega^{-\sigma}$$

instead of complete exponential suppression at large frequencies. Our networks generated algebraically persistent spectral intensities together with scale-dependent spectral incompatibility extending across large scales.

These persistence laws should not be interpreted as universal properties of every singular system, but as conditional predictions expected when obstruction classes are algebraically distributed across resolutions. Under these conditions, persistent singular organization generates measurable multiscale signatures differing from the fast convergence typically associated with smooth-field regularization.

Overall, we derived measurable quantities associated with persistent singular organization and established explicit scaling predictions for persistence spectra, metric fluctuations, causal propagation, topological memory and noncommutative spectral behavior. Compared with smooth exponentially regularized comparator systems, our simulated networks consistently generated algebraic persistence, residual metric fluctuations, broadened causal propagation, long-range memory correlations and persistent spectral incompatibility.

5. Conclusion

We investigated the possibility that persistent singular organization may provide a generative route toward effective geometry, causal propagation and quantum-like incompatibility. Relative cohomology, obstruction classes, persistence morphisms and obstruction-preserving interaction operators were used to build a mathematical description of singular persistence across scales. Smooth geometry was treated not as a primitive background structure, but as a statistical large-scale regularization emerging from deeper singular organization. Our analysis showed that collective singular interactions could generate metric organization, directed causal propagation and noncommutative observables without assuming differentiable space-time as primitive. Metric structure emerged from singular interaction statistics, while causal ordering from directed obstruction accessibility. Similarly, quantum-like incompatibility emerged from asymmetries in singular propagation ordering rather than from axiomatic canonical quantization.

Unlike approaches like causal-set theory, spin-network models, topological quantum field theory or noncommutative geometry (Johnston 2009; Takesue and Inagaki 2016; Tonielli et al. 2020; Kauffman 2022; Marcianò et al. 2022; Zache et al. 2023; Jaksland and Linnemann 2025; Iulianelli et al. 2025), the primary organizational role is assigned to persistent, non-removable singular obstruction itself. Also, we introduced explicit measurable observables associated with persistent singular organization, including persistence spectra, anomalous metric fluctuations, causal propagation exponents, topological memory correlations, noncommutative spectral intensities and residual curvature variance. A synthetic graph-based simulation of interacting singular loci embedded within a finite millimetric domain generated algebraic persistence spectra, broadened causal propagation, long-tailed topological memory, residual metric fluctuations and persistent spectral incompatibility relative to smooth exponentially regularized comparator systems.

Our approach has limitations. Our framework should not be interpreted as a finalized derivation of geometry or quantum theory. Singular interaction amplitudes, adjacency operators and propagation rules define a constrained class of admissible interaction dynamics rather than a unique microscopic law. Our analysis does not derive the full structure of quantum mechanics, gauge invariance, canonical commutation relations or the Born rule: its more limited claim is that one quantum-like feature, namely incompatibility of observables, can emerge operationally from directed

 doi:10.20944/preprints202605.1963.v1

singular propagation. Also, our proposed scaling laws should not be interpreted as universal properties of all singular systems, but as conditional predictions expected when obstruction classes are algebraically distributed across coarse-graining scales. Under strong exponential suppression, our model converges toward ordinary smooth-field behavior and singularity-specific signatures disappear.

In conclusion, we asked whether singularity can be interpreted not merely as a breakdown of physical description, but as a possible source of geometric, causal and quantum-like organization. Our analysis showed that persistent singular structures can be represented operationally through relative cohomology, obstruction persistence, singular interaction networks and coarse-grained stabilization procedures, while simultaneously generating explicit measurable observables and computationally reproducible scaling relations. Within our perspective, smooth geometry stands for a statistical large-scale manifestation of deeper non-removable singular organization rather than a primary substrate underlying singular structures.

Ethics approval and consent to participate: This research does not contain any studies with human participants or animals performed by the Author.

Consent for publication: The Author transfers all copyright ownership in the event the work is published. The undersigned author warrants that the article is original, does not infringe on any copyright or other proprietary right of any third part, is not under consideration by another journal and has not been previously published.

Availability of data and materials: All data and materials generated or analyzed during this study are included in the manuscript. The Author had full access to all the data in the study and took responsibility for the integrity of the data and the accuracy of the data analysis.

Disclaimer: The views expressed are those of the author and do not necessarily reflect those of the affiliated institutions.

Competing interests: The Author does not have any known or potential conflict of interest including any financial, personal or other relationships with other people or organizations within three years of beginning the submitted work that could inappropriately influence or be perceived to influence their work.

Funding: This research did not receive any specific grant from funding agencies in the public, commercial or not-for-profit sectors.

Acknowledgments: none.

Authors' contributions: The Author performed: study concept and design, acquisition of data, analysis and interpretation of data, drafting of the manuscript, critical revision of the manuscript for important intellectual content, statistical analysis, obtained funding, administrative, technical and material support, study supervision.

Declaration of generative AI and AI-assisted technologies in the writing process: During the preparation of this work, the author used ChatGPT 5.3 to assist with data analysis and manuscript drafting and to improve spelling, grammar and general editing. After using this tool, the author reviewed and edited the content as needed, taking full responsibility for the content of the publication.

References

1. Aubry, S. 2026. "General Relativity in Flat Space-Time." Chaos 36 (4): 043110. https://doi.org/10.1063/5.0285341.
2. Bern, Z., C. Cheung, H. H. Chi, S. Davies, L. Dixon, and J. Nohle. 2015. "Evanescent Effects Can Alter Ultraviolet Divergences in Quantum Gravity without Physical Consequences." Physical Review Letters 115 (21): 211301. https://doi.org/10.1103/PhysRevLett.115.211301.
3. Chatton, E., T. Labasque, J. de La Bernardie, N. Guihéneuf, O. Bour, and L. Aquilina. 2017. "Field Continuous Measurement of Dissolved Gases with a CF-MIMS: Applications to the Physics and Biogeochemistry of Groundwater Flow." Environmental Science and Technology 51 (2): 846–854. https://doi.org/10.1021/acs.est.6b03706.

 doi:10.20944/preprints202605.1963.v1

4. Chikayama, E. 2014. “Decomposition of Multivariate Function Using the Heaviside Step Function.” SpringerPlus 3: 704. https://doi.org/10.1186/2193-1801-3-704.
5. Endresen, K. D., M. Kim, M. Pittman, Y. Chen, and F. Serra. 2021. “Topological Defects of Integer Charge in Cell Monolayers.” Soft Matter 17 (24): 5878–5887. https://doi.org/10.1039/d1sm00100k.
6. Fernández-Jambrina, L., and R. Lazkoz. 2022. “New Futures for Cosmological Models.” Philosophical Transactions of the Royal Society A: Mathematical, Physical and Engineering Sciences 380 (2222): 20210333. https://doi.org/10.1098/rsta.2021.0333.
7. Gao, Z., S. W. Cheong, and X. Wang. 2025. “Ferroelectric Topological Defects in Hexagonal Manganites.” Materials 19 (1): 31. https://doi.org/10.3390/ma19010031.
8. Grusdt, F., N. Mostaan, E. Demler, and L. A. P. Ardila. 2025. “Impurities and Polarons in Bosonic Quantum Gases: A Review on Recent Progress.” Reports on Progress in Physics 88 (6). https://doi.org/10.1088/1361-6633/add94b.
9. Han, I. S. 2025. “Analysis of Electric Field in Inclined Dielectric Media by Heaviside Unit-Step Function.” Scientific Reports 15 (1): 13066. https://doi.org/10.1038/s41598-025-97716-7.
10. Iacovelli, G., and C. Iacovelli. 2022. “Representing Logic Gates over Euclidean Space via Heaviside Step Function.” Scientific Reports 12 (1): 8009. https://doi.org/10.1038/s41598-022-11941-y.
11. Iulianelli, F., S. Kim, J. Sussan, and A. D. Lauda. 2025. “Universal Quantum Computation Using Ising Anyons from a Non-Semisimple Topological Quantum Field Theory.” Nature Communications 16 (1): 6408. https://doi.org/10.1038/s41467-025-61342-8.
12. Jaksland, R., and N. Linnemann. 2025. “On the Non-identity Causal Theory of Spacetime from Causal Set Theory.” Erkenntnis 90 (8): 3425–3446. https://doi.org/10.1007/s10670-024-00836-1.
13. Johnston, S. 2009. “Feynman Propagator for a Free Scalar Field on a Causal Set.” Physical Review Letters 103 (18): 180401. https://doi.org/10.1103/PhysRevLett.103.180401.
14. Kauffman, S. A. 2022. “Quantum Gravity If Non-Locality Is Fundamental.” Entropy 24 (4): 554. https://doi.org/10.3390/e24040554.
15. Mains, A. J., J. X. Zhong, Y. Jing, and B. Roy. 2026. “Ordinary Lattice Defects as Probes of Topology.” Reports on Progress in Physics 89 (4). https://doi.org/10.1088/1361-6633/ae5bcb.
16. Marcianò, A., D. Chen, F. Fabrocini, C. Fields, E. Greco, N. Gresnigt, K. Jinklub, M. Lulli, K. Terzidis, and E. Zappala. 2022. “Quantum Neural Networks and Topological Quantum Field Theories.” Neural Networks 153: 164–178. https://doi.org/10.1016/j.neunet.2022.05.028.
17. McKerral, J. C., M. Kleshnina, V. Ejov, L. Bartle, J. G. Mitchell, and J. A. Filar. 2023. “Empirical Parameterisation and Dynamical Analysis of the Allometric Rosenzweig-MacArthur Equations.” PLoS ONE 18 (2): e0279838. https://doi.org/10.1371/journal.pone.0279838.
18. Nabeel, A., V. Jadhav, M. DR, C. Sire, G. Theraulaz, R. Escobedo, S. K. Iyer, and V. Guttal. 2023. “Data-Driven Discovery of Stochastic Dynamical Equations of Collective Motion.” Physical Biology 20 (5). https://doi.org/10.1088/1478-3975/ace22d.
19. Palmer, B., S. Chen, P. Govan, W. Yan, and T. Gao. 2022. “Understanding Topological Defects in Fluidized Dry Active Nematics.” Soft Matter 18 (5): 1013–1018. https://doi.org/10.1039/d1sm01405f.
20. Shankar, S., L. V. D. Scharrer, M. J. Bowick, and M. C. Marchetti. 2024. “Design Rules for Controlling Active Topological Defects.” Proceedings of the National Academy of Sciences of the United States of America 121 (21): e2400933121. https://doi.org/10.1073/pnas.2400933121.
21. Slepukhin, V. M., M. J. Grill, Q. Hu, E. L. Botvinick, W. A. Wall, and A. J. Levine. 2021. “Topological Defects Produce Kinks in Biopolymer Filament Bundles.” Proceedings of the National Academy of Sciences of the United States of America 118 (15): e2024362118. https://doi.org/10.1073/pnas.2024362118.
22. Steinbauer, R. 2023. “The Singularity Theorems of General Relativity and Their Low Regularity Extensions.” Jahresbericht der Deutschen Mathematiker-Vereinigung 125 (2): 73–119. https://doi.org/10.1365/s13291-022-00263-7.
23. Takesue, H., and T. Inagaki. 2016. “10 GHz Clock Time-Multiplexed Degenerate Optical Parametric Oscillators for a Photonic Ising Spin Network.” Optics Letters 41 (18): 4273–4276. https://doi.org/10.1364/OL.41.004273.

 doi:10.20944/preprints202605.1963.v1

24. Tonielli, F., J. C. Budich, A. Altland, and S. Diehl. 2020. "Topological Field Theory Far from Equilibrium." Physical Review Letters 124 (24): 240404. https://doi.org/10.1103/PhysRevLett.124.240404.
25. Tzitzimpasis, P., M. Ries, B. W. Raaymakers, and C. Zachiu. 2024. "Generalized Div-Curl Based Regularization for Physically Constrained Deformable Image Registration." Scientific Reports 14 (1): 15002. https://doi.org/10.1038/s41598-024-65896-3.
26. Wotte, Y. P., F. Califano, and S. Stramigioli. 2025. "Geometric Neural Ordinary Differential Equations: From Manifolds to Lie Groups." Entropy 27 (8): 878. https://doi.org/10.3390/e27080878.
27. Wu, K. H., Z. Sun, L. T. Zhu, S. S. Li, X. Hu, Q. H. Liu, and L. J. Chen. 2026. "Harnessing Acoustic Topology for Dynamic Control of Liquid Crystal Defects." Nature Communications 17 (1): 1242. https://doi.org/10.1038/s41467-025-68001-y.
28. Zache, T. V., D. González-Cuadra, and P. Zoller. 2023. "Quantum and Classical Spin-Network Algorithms for q-Deformed Kogut-Susskind Gauge Theories." Physical Review Letters 131 (17): 171902. https://doi.org/10.1103/PhysRevLett.131.171902.